Electron Neutrino and Antineutrino Appearance in the Full MINOS Data Sample

P. Adamson,[8] I. Anghel,[1,15] C. Backhouse,[21] G. Barr,[21] M. Bishai,[3] A. Blake,[5] G. J. Bock,[8] D. Bogert,[8] S. V. Cao,[29]
D. Cherdack,[30] S. Childress,[8] J. A. B. Coelho,[30,6] L. Corwin,[14] D. Cronin-Hennessy,[18] J. K. de Jong,[21] A. V. Devan,[32]
N. E. Devenish,[27] M. V. Diwan,[3] C. O. Escobar,[6] J. J. Evans,[17,16] E. Falk,[27] G. J. Feldman,[10] M. V. Frohne,[11]
H. R. Gallagher,[30] R. A. Gomes,[9] M. C. Goodman,[1] P. Gouffon,[24] N. Graf,[13] R. Gran,[19] K. Grzelak,[31] A. Habig,[19]
S. R. Hahn,[8] J. Hartnell,[27] R. Hatcher,[8] A. Himmel,[4] A. Holin,[16] J. Hylen,[8] G. M. Irwin,[26] Z. Isvan,[3,22] D. E. Jaffe,[3]
C. James,[8] D. Jensen,[8] T. Kafka,[30] S. M. S. Kasahara,[18] G. Koizumi,[8] M. Kordosky,[32] A. Kreymer,[8] K. Lang,[29] J. Ling,[3]
P. J. Litchfield,[18,23] P. Lucas,[8] W. A. Mann,[30] M. L. Marshak,[18] M. Mathis,[32] N. Mayer,[30,14] M. M. Medeiros,[9]
R. Mehdiyev,[29] J. R. Meier,[18] M. D. Messier,[14] D. G. Michael,[4,*] W. H. Miller,[18] S. R. Mishra,[25] S. Moed Sher,[8]
C. D. Moore,[8] L. Mualem,[4] J. Musser,[14] D. Naples,[22] J. K. Nelson,[32] H. B. Newman,[4] R. J. Nichol,[16] J. A. Nowak,[18]
J. P. Ochoa-Ricoux,[4] J. O'Connor,[16] W. P. Oliver,[30] M. Orchanian,[4] R. B. Pahlka,[8] J. Paley,[1] R. B. Patterson,[4]
G. Pawloski,[18,26] S. Phan-Budd,[1] R. K. Plunkett,[8] X. Qiu,[26] A. Radovic,[16] B. Rebel,[8] C. Rosenfeld,[25] H. A. Rubin,[13]
M. C. Sanchez,[15,1] J. Schneps,[30] A. Schreckenberger,[18] P. Schreiner,[1] R. Sharma,[8] A. Sousa,[7,10] N. Tagg,[20] R. L. Talaga,[1]
J. Thomas,[16] M. A. Thomson,[5] G. Tinti,[21] R. Toner,[10,5] D. Torretta,[8] G. Tzanakos,[2] J. Urheim,[14] P. Vahle,[32] B. Viren,[3]
A. Weber,[21,23] R. C. Webb,[28] C. White,[13] L. Whitehead,[12,3] S. G. Wojcicki,[26] T. Yang,[26] and R. Zwaska[8]

(MINOS Collaboration)

[1]*Argonne National Laboratory, Argonne, Illinois 60439, USA*
[2]*Department of Physics, University of Athens, GR-15771 Athens, Greece*
[3]*Brookhaven National Laboratory, Upton, New York 11973, USA*
[4]*Lauritsen Laboratory, California Institute of Technology, Pasadena, California 91125, USA*
[5]*Cavendish Laboratory, University of Cambridge, Madingley Road, Cambridge CB3 0HE, United Kingdom*
[6]*Universidade Estadual de Campinas, IFGW-UNICAMP, CP 6165, 13083-970, Campinas, SP, Brazil*
[7]*Department of Physics, University of Cincinnati, Cincinnati, Ohio 45221, USA*
[8]*Fermi National Accelerator Laboratory, Batavia, Illinois 60510, USA*
[9]*Instituto de Física, Universidade Federal de Goiás, CP 131, 74001-970, Goiânia, GO, Brazil*
[10]*Department of Physics, Harvard University, Cambridge, Massachusetts 02138, USA*
[11]*Holy Cross College, Notre Dame, Indiana 46556, USA*
[12]*Department of Physics, University of Houston, Houston, Texas 77204, USA*
[13]*Department of Physics, Illinois Institute of Technology, Chicago, Illinois 60616, USA*
[14]*Indiana University, Bloomington, Indiana 47405, USA*
[15]*Department of Physics and Astronomy, Iowa State University, Ames, Iowa 50011, USA*
[16]*Department of Physics and Astronomy, University College London, Gower Street, London WC1E 6BT, United Kingdom*
[17]*School of Physics and Astronomy, University of Manchester, Oxford Road, Manchester M13 9PL, United Kingdom*
[18]*University of Minnesota, Minneapolis, Minnesota 55455, USA*
[19]*Department of Physics, University of Minnesota Duluth, Duluth, Minnesota 55812, USA*
[20]*Otterbein University, Westerville, Ohio 43081, USA*
[21]*Subdepartment of Particle Physics, University of Oxford, Oxford OX1 3RH, United Kingdom*
[22]*Department of Physics and Astronomy, University of Pittsburgh, Pittsburgh, Pennsylvania 15260, USA*
[23]*Rutherford Appleton Laboratory, Science and Technologies Facilities Council, Harwell, Didcot OX11 0QX, United Kingdom*
[24]*Instituto de Física, Universidade de São Paulo, CP 66318, 05315-970, São Paulo, SP, Brazil*
[25]*Department of Physics and Astronomy, University of South Carolina, Columbia, South Carolina 29208, USA*
[26]*Department of Physics, Stanford University, Stanford, California 94305, USA*
[27]*Department of Physics and Astronomy, University of Sussex, Falmer, Brighton BN1 9QH, United Kingdom*
[28]*Physics Department, Texas A&M University, College Station, Texas 77843, USA*
[29]*Department of Physics, University of Texas at Austin, 1 University Station C1600, Austin, Texas 78712, USA*
[30]*Physics Department, Tufts University, Medford, Massachusetts 02155, USA*
[31]*Department of Physics, University of Warsaw, Hoża 69, PL-00-681 Warsaw, Poland*
[32]*Department of Physics, College of William & Mary, Williamsburg, Virginia 23187, USA*

We report on ν_e and $\bar{\nu}_e$ appearance in ν_μ and $\bar{\nu}_\mu$ beams using the full MINOS data sample. The
comparison of these ν_e and $\bar{\nu}_e$ appearance data at a 735 km baseline with θ_{13} measurements by reactor
experiments probes δ, the θ_{23} octant degeneracy, and the mass hierarchy. This analysis is the first use of
this technique and includes the first accelerator long-baseline search for $\bar{\nu}_\mu \rightarrow \bar{\nu}_e$. Our data disfavor 31%

(5%) of the three-parameter space defined by δ, the octant of the θ_{23}, and the mass hierarchy at the 68%
(90%) C.L. We measure a value of $2\sin^2(2\theta_{13})\sin^2(\theta_{23})$ that is consistent with reactor experiments.

The neutrino oscillation phenomenon is successfully modeled by a theory of massive neutrino eigenstates that are different from the neutrino flavor eigenstates. These sets of eigenstates are related by the Pontecorvo-Maki-Nakagawa-Sakata matrix [1], which is commonly parametrized by three angles θ_{ij} and a *CP*-violating phase δ.

The values of θ_{12} and θ_{23} have been measured [2–4] with indications that θ_{23} is not maximal [5–7]. The final angle θ_{13} is now known to have a nonzero value from measurements by reactor experiments [8–10], the measurement by the T2K [11] accelerator experiment, and from earlier MINOS results [12,13].

Despite these accomplishments, the value of δ is still unknown, as is the ordering of the neutrino masses, which is referred to as the neutrino mass hierarchy. Much of the attention in the neutrino community is now focused on resolving these unknowns. The mass hierarchy is not only a fundamental property of neutrinos but also has a direct impact on the ability of neutrinoless double beta decay searches to state definitively whether the neutrino is its own antiparticle [14]. Reactor experiments make a pure measurement of θ_{13}, whereas the $\nu_\mu \rightarrow \nu_e$ and $\bar{\nu}_\mu \rightarrow \bar{\nu}_e$ appearance probabilities measured by accelerator experiments such as MINOS depend on the values of δ and $\sin^2(\theta_{23})$. In addition, the long baseline of MINOS means that interactions between neutrinos and the matter of Earth make the appearance probabilities dependent on the neutrino mass hierarchy [15,16].

We report the result from the search for ν_e ($\bar{\nu}_e$) appearance in a ν_μ ($\bar{\nu}_\mu$) beam using the full MINOS data sample. This result uses an exposure of 10.6×10^{20} protons on target (POT) taken with a ν beam and an exposure of 3.3×10^{20} POT taken with a $\bar{\nu}$ beam. The neutrino sample is 30% larger than the sample used for the previous MINOS results on this topic [13]. This analysis represents the first long-baseline search for the $\bar{\nu}_\mu \rightarrow \bar{\nu}_e$ appearance and places new constraints on θ_{13} and on a combination of δ, θ_{23}, and the neutrino mass hierarchy.

In the MINOS experiment [17], neutrino oscillation is studied with the NuMI beam line [18] by measuring neutrino interactions in two detectors. The near detector (ND), which has a fiducial mass of 29 tons, is at a distance of 1.04 km from the production target and is used to determine the composition of the beam before the neutrinos have oscillated. The far detector (FD), which has a fiducial mass of 3.8 kt, is at a distance of 735 km from the production target and is used to measure the change in the neutrino flavor composition of the beam. In both the ν and $\bar{\nu}$ beam modes, the NuMI beam has an energy spectrum that is peaked at 3 GeV. At the ND, the neutrino flavor composition of the neutrino interactions, as determined by a combination of simulation and measurement, is found to be 91.7% ν_μ, 7.0% $\bar{\nu}_\mu$, and 1.3% ν_e and $\bar{\nu}_e$ for the ν beam mode and 58.1% ν_μ, 39.9% $\bar{\nu}_\mu$, and 2.0% ν_e and $\bar{\nu}_e$ for the $\bar{\nu}$ beam mode.

Both detectors are magnetized tracking calorimeters consisting of alternating planes of 2.54 cm thick steel and 1 cm thick scintillating plastic [17]. The scintillator planes are segmented into 4.1 cm wide strips with wavelength-shifting fibers embedded in the strips to collect light for readout by multianode photomultiplier tubes.

In the MINOS data sample, the flavor of a neutrino is determined only for charged-current (CC) interactions. ν_μ-CC and $\bar{\nu}_\mu$-CC interactions are identified by the presence of a long muon track that extends beyond a cluster of energy depositions that are consistent with hadronic activity at the interaction vertex. Neutral-current (NC) interactions are identified by the energy depositions associated with hadronic activity. ν_e-CC and $\bar{\nu}_e$-CC interactions produce an electromagnetic shower that typically leaves a compact cluster within 6 to 12 planes. This analysis does not distinguish between ν_e-CC and $\bar{\nu}_e$-CC interactions.

The sample of events classified as ν_e-CC and $\bar{\nu}_e$-CC interactions contains a background of interactions with similar topology as required for ν_e-CC and $\bar{\nu}_e$-CC classification. NC interactions with a significant electromagnetic component and ν_μ-CC or $\bar{\nu}_\mu$-CC interactions in which the muon track is not easily identified make up the majority of the background. Smaller contributions to the background arise from ν_τ-CC and $\bar{\nu}_\tau$-CC interactions. In addition to backgrounds that mimic ν_e-CC and $\bar{\nu}_e$-CC event topologies, intrinsic ν_e and $\bar{\nu}_e$ components of the NuMI beam must be taken into account.

Candidate ν_e-CC and $\bar{\nu}_e$-CC events are required to fall within a fiducial volume and to be coincident in time and direction with the NuMI beam. We require the events to have showerlike topologies by rejecting events with tracks that are longer than 25 planes or extend more than 15 planes from a shower edge. In addition, reconstructed events must have at least five consecutive planes with deposited energy above a threshold; this threshold is defined as half of the energy deposited by a minimum ionizing particle. We require the events to have a reconstructed energy between 1 and 8 GeV where most of the ν_e and $\bar{\nu}_e$ appearance is expected.

We further classify the events in this preselected sample of showerlike events by using a library-event-matching (LEM) algorithm [19,20]. Within the LEM algorithm, the topology of energy depositions that characterize the event is compared to a library of simulated signal and

background events. Separate libraries are used for the
events in the ν beam mode and the $\bar{\nu}$ beam mode. The
50 best-matching events in the library are collected and
used to produce three variables. These variables are the
fraction of best-matching library events that are ν_e-CC or
$\bar{\nu}_e$-CC, the average inelasticity of the best-matching ν_e-CC
or $\bar{\nu}_e$-CC library events, and the average fraction of the
energy depositions that overlap between the test event and
the best-matching ν_e-CC or $\bar{\nu}_e$-CC library events. These
three variables and the reconstructed neutrino energy of
the test event are then used as an input into an artificial
neural network. The output value from the neural network
is used to discriminate between signal and background
events. This discriminant variable is referred to as α_{LEM}
and is shown in Fig. 1. Signal events have a value near one,
while background events cluster near zero. The maximum
sensitivity to ν_e and $\bar{\nu}_e$ appearance is obtained by analyz-
ing events with $\alpha_{\text{LEM}} > 0.6$.

Following the selection of ν_e-CC and $\bar{\nu}_e$-CC candidate
events, the ND data are used to study the rate of back-
ground from NC, ν_μ-CC and $\bar{\nu}_\mu$-CC, and intrinsic beam
ν_e-CC and $\bar{\nu}_e$-CC interactions. The NuMI beam can be
tuned to produce different energy spectra. Among these
different beam configurations, the relative contributions of
the various backgrounds change in a well-understood way.
By measuring the total of the three backgrounds in three
different beam configurations, the relative amounts of the
individual backgrounds can be deduced [21].

We use the measurement of the ND backgrounds to
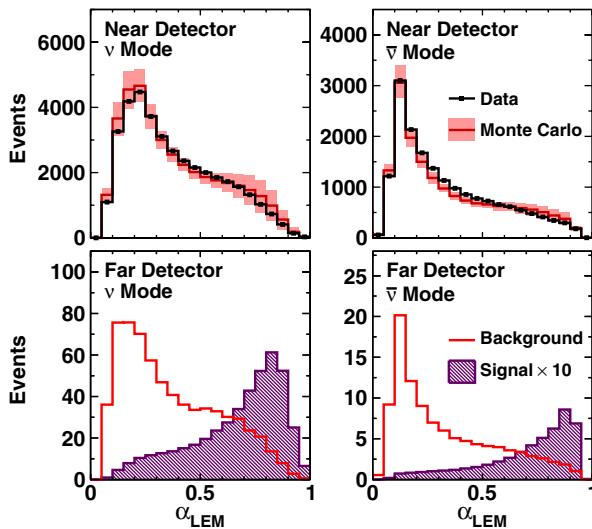derive the FD background predictions for the data samples

FIG. 1 (color online). Distributions of α_{LEM}. The plots in the
left column correspond to the ν beam mode. The plots in the
right column correspond to the $\bar{\nu}$ beam mode. The top row shows
the distributions for ND selected events with a band about the
simulation representing the systematic uncertainty. The bottom
row shows the distributions for the predicted FD background and
signal multiplied by 10 with $2\sin^2(2\theta_{13})\sin^2(\theta_{23}) = 0.1$, $\delta = 0$,
and a normal mass hierarchy.

in the ν beam mode and in the $\bar{\nu}$ beam mode. For each
sample, we divide simulated FD events into bins of energy
and α_{LEM} and correct each FD background component,
bin by bin, by multiplying it by the measured ND ratio of
data to simulated events for that background. Since the
ND data sample does not contain ν_τ-CC and $\bar{\nu}_\tau$-CC events
from oscillation, we estimate the FD contribution from
this small background component through simulation
and a correction based on the observed ND ν_μ-CC and
$\bar{\nu}_\mu$-CC spectra.

The sources of systematic uncertainty that affect the
background prediction are given in Table I. The effect of
each source of uncertainty is evaluated by producing simu-
lated ND and FD event samples that are modified accord-
ing to the estimated size of each systematic effect. These
modified samples are used to produce an altered FD back-
ground prediction for the systematic effect in question.
We take the resulting difference between the nominal and
modified predictions as the systematic uncertainty on the
background prediction. The systematic effect that results in
the largest reduction in sensitivity is a 2.0% uncertainty on
the relative energy scale between the ND and the FD.

With the absence of a ν_e-CC and $\bar{\nu}_e$-CC signal in the
ND, the signal selection efficiency cannot be extrapolated
from the ND events in the same way as the background
estimate. Therefore, to evaluate the signal efficiency, we
select a sample of well-identified ν_μ-CC events [22,23],
remove the energy depositions that are associated with the
muon track [24], and insert the simulated energy deposi-
tions of an electron with an identical three-momentum
[25]. This method effectively turns a well-identified
sample of ν_μ-CC and $\bar{\nu}_\mu$-CC data events into a sample
of ν_e-CC and $\bar{\nu}_e$-CC data events. For the ν beam mode
($\bar{\nu}$ beam mode) data sample, we find the expected number
of FD signal events with $\alpha_{\text{LEM}} > 0.6$ and the associated
systematic uncertainty to be 33.7 ± 1.9 (3.9 ± 0.2), assum-
ing $\sin^2(2\theta_{13}) = 0.1$, $\delta = 0$, $\theta_{23} = \pi/4$, and a normal mass
hierarchy. This corresponds to an identification efficiency
of $(57.4 \pm 2.8)\%$ for the ν beam mode and of $(63.3 \pm 3.1)\%$
for the $\bar{\nu}$ beam mode. The systematic uncertainties are
evaluated in a way that is similar to the evaluation of the

TABLE I. Systematic uncertainty on the FD background pre-
diction for events with a value of $\alpha_{\text{LEM}} > 0.6$. The effects listed
for "All others" include the neutrino flux, cross sections, detec-
tor modeling, and background decomposition.

Systematic effect	Uncertainty ν mode	Uncertainty $\bar{\nu}$ mode
Energy scale	2.7%	3.0%
Normalization	1.9%	1.9%
ν_τ cross section	1.7%	2.0%
All others	0.8%	2.5%
Total systematic	3.8%	4.8%
Total statistical	8.8%	23.9%

TABLE II. Expected FD event yields for events with a value of $\alpha_{LEM} > 0.6$, assuming $\sin^2(2\theta_{13}) = 0.1$, $\delta = 0$, $\theta_{23} = \pi/4$, and a normal mass hierarchy.

Event type	ν beam mode	$\bar{\nu}$ beam mode
NC	89.4	13.9
ν_μ-CC and $\bar{\nu}_\mu$-CC	21.6	1.0
Intrinsic ν_e-CC and $\bar{\nu}_e$-CC	11.9	1.8
ν_τ-CC and $\bar{\nu}_\tau$-CC	4.8	0.8
$\nu_\mu \rightarrow \nu_e$-CC	33.0	0.7
$\bar{\nu}_\mu \rightarrow \bar{\nu}_e$-CC	0.7	3.2
Total	161.4	21.4
Data	152	20

background systematics by using simulated samples that have been altered by a systematic effect.

Events with $\alpha_{LEM} < 0.5$ are insensitive to the ν_e and $\bar{\nu}_e$ appearance. These events are therefore used in a separate study to validate the analysis procedure. ND events with $\alpha_{LEM} < 0.5$ are used to predict FD event yields, which are found to agree with the FD data to within 0.3 (0.6) standard deviations of the statistical uncertainty for the data sample in the ν ($\bar{\nu}$) beam mode.
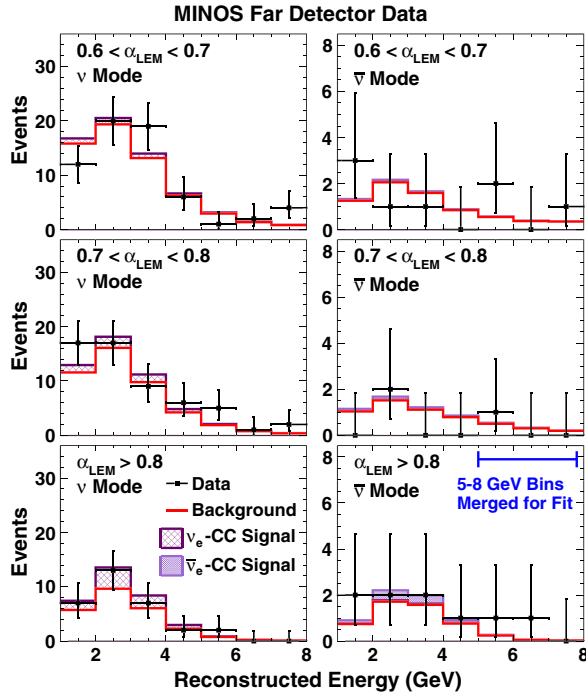
Events with $\alpha_{LEM} > 0.6$ are selected for further analysis in the ν beam mode and in the $\bar{\nu}$ beam mode. The expected and observed event counts in these samples are shown in Table II. The observed FD reconstructed energy spectra, in bins of α_{LEM}, are shown for the candidate events in Fig. 2. Assuming a three-flavor neutrino oscillation probability that includes matter effects [16], we simultaneously fit the data from the ν beam mode and $\bar{\nu}$ beam mode samples for the value of $2\sin^2(2\theta_{13})\sin^2(\theta_{23})$ while the values of the mass hierarchy and δ are held fixed. The fit is performed using the 15 bins formed by three bins of α_{LEM} and five bins of energy. This procedure is performed for all values of δ and both mass hierarchies, and the resulting confidence intervals, calculated using the Feldman-Cousins technique [26], are shown in Fig. 3. The values of the oscillation parameters used in the fit are taken from previous measurements [2,4] and are set to $\sin^2(2\theta_{23}) = 0.957^{+0.035}_{-0.036}$, $|\Delta m^2_{32}| = (2.39^{+0.09}_{-0.10}) \times 10^{-3}$ eV^2, $\theta_{12} = 0.60 \pm 0.02$, and $\Delta m^2_{21} = (7.59^{+0.19}_{-0.21}) \times 10^{-5}$ eV^2. The full set of statistical and systematic uncertainties on the prediction is taken into account when constructing the contours.

Assuming a normal mass hierarchy, $\delta = 0$, and $\theta_{23} < \pi/4$, we find that the data allow for values of $0.01 < 2\sin^2(2\theta_{13})\sin^2(\theta_{23}) < 0.12$ at 90% C.L. with the best-fit value of $2\sin^2(2\theta_{13})\sin^2(\theta_{23}) = 0.051^{+0.038}_{-0.030}$. Assuming an
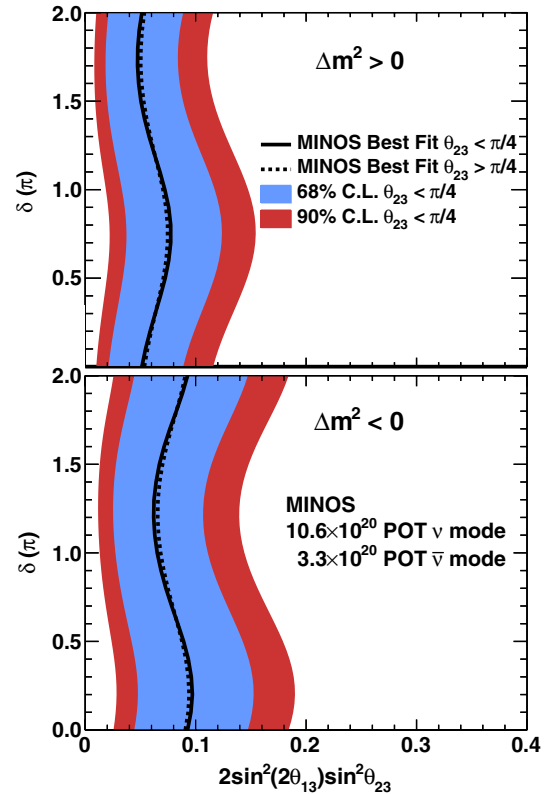

FIG. 2 (color online). The reconstructed energy distributions for three α_{LEM} ranges. The events with energy greater than 5 GeV are combined into a single bin for the fits. The vertical bars through the data points denote statistical uncertainties. The signal predictions assume $\sin^2(2\theta_{13}) = 0.051$, $\Delta m^2_{32} > 0$, $\delta = 0$, and $\theta_{23} = \pi/4$. The plots in the left column correspond to data collected in the ν beam mode. The plots in the right column correspond to data collected in the $\bar{\nu}$ beam mode.

FIG. 3 (color online). The 68% and 90% confidence intervals of allowed values for $2\sin^2(2\theta_{13})\sin^2\theta_{23}$ as a function of δ for the two mass hierarchies.
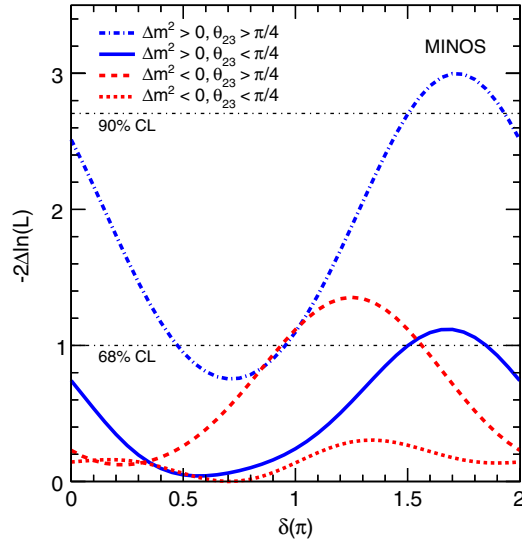
FIG. 4 (color online).   The resulting values of the likelihood L, shown here as $-2\Delta \ln L$, from a fit of δ to our data using constraints from reactor experiments [8–10], assuming various values of the mass hierarchy and the sign of $\theta_{23} - \pi/4$. The difference is taken with respect to the best-fitting solution. Values above the horizontal dashed lines are disfavored at either 68% or 90% C.L.

inverted mass hierarchy, $\delta = 0$, and $\theta_{23} < \pi/4$, we find that the data allow for values of $0.03 < 2\sin^2(2\theta_{13})\sin^2(\theta_{23}) < 0.18$ at 90% C.L. with the best-fit value of $2\sin^2(2\theta_{13})\sin^2(\theta_{23}) = 0.093^{+0.054}_{-0.049}$. The best-fit values show very weak dependence on the choice of octant for θ_{23}.

We are further able to place constraints on the value of δ, the octant of θ_{23}, and the neutrino mass hierarchy by incorporating the current knowledge of $\sin^2(2\theta_{13}) = 0.098 \pm 0.013$ that we calculate from recent reactor data [8–10]. Figure 4 shows the likelihood for our data as a function of δ for the four possible combinations of mass hierarchy and the octant of θ_{23}. The full set of statistical and systematic uncertainties on the prediction is taken into account when calculating the likelihood, as are the uncertainties on the oscillation parameters. This analysis represents the first result by a long-baseline experiment to use a combination of $\nu_\mu \rightarrow \nu_e$ and $\bar{\nu}_\mu \rightarrow \bar{\nu}_e$ appearance data, with external reactor constraints on θ_{13}, to probe δ, the θ_{23} octant degeneracy, and the mass hierarchy. Assuming $\theta_{23} > \pi/4$ ($\theta_{23} < \pi/4$), the data prefer an inverted hierarchy at 0.63 (0.04) units of $-2\Delta \ln L$. Furthermore, as is indicated by the horizontal lines in Fig. 4, our data disfavor 31% (5%) of the three-parameter space defined by δ, the octant of the θ_{23}, and the mass hierarchy at the 68% (90%) C.L. This analysis demonstrates the potential discriminating power that can be achieved with the combination of reactor and $\nu_\mu \rightarrow \nu_e$ and $\bar{\nu}_\mu \rightarrow \bar{\nu}_e$ appearance data.

In conclusion, we have presented the results of the ν_e and $\bar{\nu}_e$ appearance in ν_μ and $\bar{\nu}_\mu$ beams from the full MINOS data sample. We have used these data to place new constraints on the mixing angle θ_{13} and have demonstrated how such data will be used in the future to break the degeneracy in the appearance probability created by the ambiguity in the octant of θ_{23}, the neutrino mass hierarchy, and the value of the *CP*-violating phase δ.

*Deceased.
[1] B. Pontecorvo, Zh. Eksp. Teor. Fiz. **34**, 247 (1957) [Sov. Phys. JETP **7**, 172 (1958)]; V. N. Gribov and B. Pontecorvo, Phys. Lett. **28B**, 493 (1969); Z. Maki, M. Nakagawa, and S. Sakata, Prog. Theor. Phys. **28**, 870 (1962).
[2] B. Aharmim *et al.* (SNO Collaboration), Phys. Rev. Lett. **101**, 111301 (2008).
[3] Y. Ashie *et al.* (Super-Kamiokande Collaboration), Phys. Rev. D **71**, 112005 (2005).
[4] R. Nichol, in Proceedings of the XXV International Conference on Neutrino Physics and Astrophysics, Kyoto, Japan, 2012 (Elsevier, Amsterdam, to be published).
[5] G. L. Fogli, E. Lisi, A. Marrone, D. Montanino, A. Palazzo, and A. M. Rotunno, Phys. Rev. D **86**, 013012 (2012).
[6] M. C. Gonzalez-Garcia, M. Maltoni, J. Salvado, and T. Schwetz, J. High Energy Phys. 12 (2012) 123.
[7] Y. Itow, in Proceedings of the XXV International Conference on Neutrino Physics and Astrophysics, Kyoto, Japan, 2012 (Elsevier, Amsterdam, to be published).
[8] Y. Abe *et al.* (Double Chooz Collaboration), Phys. Rev. Lett. **108**, 131801 (2012).
[9] F. P. An *et al.* (Daya Bay Collaboration), Phys. Rev. Lett. **108**, 171803 (2012).
[10] J. K. Ahn *et al.* (RENO Collaboration), Phys. Rev. Lett. **108**, 191802 (2012).
[11] K. Abe *et al.* (T2K Collaboration), Phys. Rev. Lett. **107**, 041801 (2011).
[12] P. Adamson *et al.* (MINOS Collaboration), Phys. Rev. Lett. **103**, 261802 (2009); Phys. Rev. D **82**, 051102(R) (2010).
[13] P. Adamson *et al.* (MINOS Collaboration), Phys. Rev. Lett. **107**, 181802 (2011).
[14] J. Beringer *et al.* (Particle Data Group), Phys. Rev. D **86**, 010001 (2012).
[15] L. Wolfenstein, Phys. Rev. D **17**, 2369 (1978); S. P. Mikheyev and A. Yu. Smirnov, Yad. Fiz. **42**, 1441 (1985) [Sov. J. Nucl. Phys. **42**, 913 (1985)].
[16] E. K. Akhmedov, R. Johansson, M. Lindner, T. Ohlsson, and T. Schwetz, J. High Energy Phys. 04 (2004) 078.

[17] D. G. Michael *et al.* (MINOS Collaboration), Nucl. Instrum. Methods Phys. Res., Sect. A **596,** 190 (2008).

[18] K. Anderson *et al.*, Fermilab Report No. FERMILAB-DESIGN-1998-01, 1998 (unpublished).

[19] J. P. Ochoa, Ph.D. thesis, California Institute of Technology [Fermilab Report No. FERMILAB-THESIS-2009-44, 2009 (unpublished)].

[20] R. Toner, Ph.D. thesis, University of Cambridge [Fermilab Report No. FERMILAB-THESIS-2011-53, 2011 (unpublished)].

[21] J. A. B. Coelho, Ph.D. thesis, Universidade Estadual de Campinas [Fermilab Report No. FERMILAB-THESIS-2012-23, 2012 (unpublished)].

[22] R. Ospanov, Ph.D. thesis, University of Texas at Austin [Fermilab Report No. FERMILAB-THESIS-2008-04, 2008 (unpublished)].

[23] P. Adamson *et al.* (MINOS Collaboration), Phys. Rev. Lett. **106,** 181801 (2011).

[24] A. Holin, Ph.D. thesis, University College London [Fermilab Report No. FERMILAB-THESIS-2010-41, 2010 (unpublished)].

[25] J. Boehm, Ph.D. thesis, Harvard University [Fermilab Report No. FERMILAB-THESIS-2009-17, 2009 (unpublished)].

[26] G. J. Feldman and R. D. Cousins, Phys. Rev. D **57,** 3873 (1998).